Partitioning Behavior and Mechanisms of Rare Earth Elements during Precipitation in Acid Mine Drainage

Qi Li [1], Bin Ji [1], Rick Honaker [2], Aaron Noble [1], Wencai Zhang [1, *]

[1] *Department of Mining and Minerals Engineering, Virginia Polytechnic Institute and State University, Blacksburg, Virginia 24061, USA*

[2] *Department of Mining Engineering, University of Kentucky, Lexington, Kentucky 40506, USA*

Abstract: Rare earth elements (REEs) are frequently found concentrated in acid mine drainage (AMD). The recovery of REEs from AMD has been successfully achieved using selective chemical precipitation. However, a portion of the REEs is often lost to the precipitates of the dominant metal contaminant ions. To better understand the REE partitioning behavior and mechanisms during the precipitation process, a systematic study was performed on both natural and synthetic AMD solutions. Precipitation test results show that REE removal was noticeably elevated at pH 4.0 after adding H_2O_2 to convert ferrous to ferric ions, causing nearly complete precipitation of iron. Solution equilibrium calculations suggested that the REE removal increase was realized through adsorption onto the surfaces of the ferric precipitates. The presence of aluminum species in the solutions reduced the adsorption of REEs on the ferric precipitates. Based on electro-kinetic test results, it was concluded that aluminum species neutralize the negative surface charge of the ferric precipitates and compete with REEs for the adsorption active sites. The presence of ferrous ions in the solutions reduced REE adsorption on the aluminum precipitates at lower pH values (e.g., 5.0) due to competitive adsorption. However, at higher pH values (e.g., 6.0), REE removal to the precipitate product increased due to the precipitation of ferrous ions. Besides the electro-kinetic tests and solution equilibrium calculations, mineralogy characterization, specific surface area measurement, particle size analysis, and morphology analysis were also conducted to reveal the partitioning mechanisms.

Keywords: Acid mine drainage, Rare earth elements, Partitioning behavior, Partitioning mechanisms

Corresponding author: W. Zhang

E-mail: wencaizhang@vt.edu

1. Introduction

Depending on the regional geology, coal mining, metal mining, and other large scale excavations can liberate sulfide minerals, like pyrite, which can in turn react with water and oxygen to form acid mine drainage (AMD) (MacIngova and Luptakova, 2012; Baleeiro et al., 2018). The chemical reactions related to AMD formation are:

$$2FeS_2 + 7O_2 + 2H_2O \rightarrow 2Fe^{2+} + 4SO_4^{2-} + 4H^+ \quad \text{Eq. (1)}$$

$$4Fe^{2+} + O_2 + 4H^+ \rightarrow 4Fe^{3+} + 2H_2O \quad \text{Eq. (2)}$$

$$4Fe^{3+} + 12H_2O \rightarrow 4Fe(OH)_3 \downarrow + 12H^+ \quad \text{Eq. (3)}$$

$$FeS_2 + 14Fe^{3+} + 8H_2O \rightarrow 15Fe^{2+} + 2SO_4^{2-} + 16H^+ \quad \text{Eq. (4)}$$

According to the reactions given above, hydrogen ions are generated during the oxidation process, and as a result, AMD normally has high acidity, elevated concentrations of dissolved metals, and high sulfate content. These properties pose a potential environmental threat to natural water quality (Wang et al., 2019; Achterberg et al., 2003; Fukushi et al., 2004). The resulting contamination of natural water sources poses a threat to both animal life and vegetation. In many jurisdictions, mining companies are obligated to capture and treat AMD, and regulations, such as Section 402 of the Clean Water Act in the U.S., dictate the permitting process for water treatment. However, in addition to the potential environmental liability, the acidic nature contributes to the appearance of valuable elements such as rare earth elements (REEs) in AMD due to the dissolution of easy-to-leach, valuable element-bearing minerals comprised in coal and sulfide ore sources. As such, AMD may be a valuable alternative source for REEs and other critical materials (Christopher R Vass et al., 2019; Christopher R. Vass et al., 2019).

As the largest chemically coherent group in the periodic table, REEs consist of lanthanides, scandium (Sc), and yttrium (Y). This group of elements, divided into light (LREE: La to Sm plus Sc) and heavy (HREE: Eu to Lu plus Y), have attracted great interest in the past several years due to their unabated growth in demand by modern technology and industry, as well as the uneven distribution of their conventional ore resources worldwide (Alonso et al., 2012; Massari and Ruberti, 2013; Sprecher et al., 2014). Being motivated by these factors, research activity has been recently accelerated to assess the feasibility of REE recovery from alternate sources, especially coal-related materials, such as coal waste and coal combustion ash (Franus et al., 2015; Zhang et al., 2020). As aforementioned, REEs are dissolved in AMD due to the acidity of AMD, and in some cases, their concentrations in AMD are several orders of magnitude higher than those in natural water (Lozano et al., 2019). Therefore, the recovery of REEs from AMD has been investigated in several studies, and various techniques have been employed, including chemical precipitation (Franus et al., 2015; Hassas et al., 2021; Zhang and Honaker, 2020, 2018), ion exchange (Felipe et al., 2020), and adsorption (Ayora et al., 2016b). A selective chemical precipitation method has been installed and tested in a rare earth pilot plant to produce high-purity rare earth products from coal-related materials (Honaker et al., 2020). In the selective chemical precipitation process (Figure 1), the pH of AMD was incrementally elevated by adding bases, and the contaminant metal ions (primarily Fe and Al) were removed while the REEs were concentrated by eliminating and collecting precipitates formed in different pH ranges, respectively.

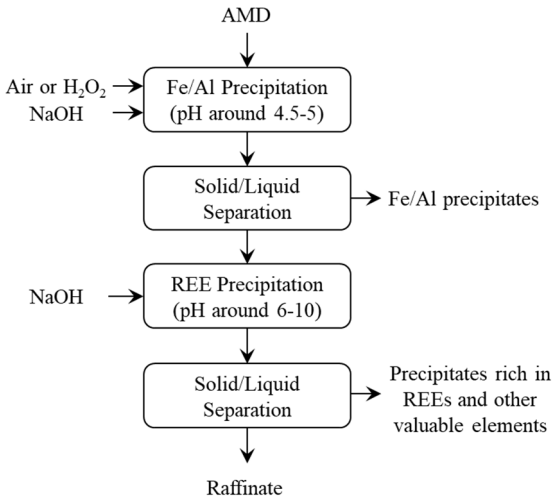

Figure 1. A selective chemical precipitation flowsheet for preconcentrating REEs and other valuable elements from AMD (Zhang and Honaker, 2020, 2018).

Large amounts of contaminant metal ions, such as iron and aluminum, are typically found in AMD. In previous studies, amorphous to semi-crystalline oxyhydroxide and hydroxysulfate precipitates of Fe and Al were present in AMD, which were likely formed during the oxidation and neutralization of AMD (Wang et al., 2021). Subject to ionic solution concentrations, a low pH range of around 2.8 to 4.5 favors iron precipitate formation, while a higher pH range leads to the formation of aluminum precipitates (Kim, 2015). According to the generation mechanisms of AMD (Eq. (1-4)), it is important to note that Fe^{2+} co-exists with Fe^{3+} in solution with additional ferric formed from the oxidation of ferrous ions followed by precipitation at low pH values (Balintova and Petrilakova, 2011; Huang and Zhou, 2012; Wei et al., 2005). The formation of these precipitates can cause the retention of REEs, thereby reducing their concentration in AMD. Therefore, this reaction is not favorable from the aspect of REE concentration in AMD. Similarly, during the selective chemical precipitation process (Figure 1), a portion of the REEs existing in AMD are also lost to the precipitates of major contaminant metal ions (e.g., Fe^{3+} and Al^{3+}). To reduce the loss, a comprehensive understanding of the partitioning behavior and mechanisms of REEs during the selective chemical precipitation process is required.

Many studies have been performed to assess the adsorption behavior and mechanisms of trace metal ions on the solids that normally form in AMD, such as (1) synthetic schwertmannite, ferrihydrite, and basaluminite minerals, (2) precipitates formed from AMD in the natural environment, and (3) precipitates formed from AMD during the passive remediation process by neutralization with calcite (Ayora et al., 2016; Lozano et al., 2019, 2020; Verplanck et al., 2004; Webster et al., 1998). The impacts of various factors, such as pH, sulfate, dominant metal ions, and other trace metal ions, on the adsorption of selected trace metal ions have been investigated. Adsorption models have been developed to simulate and explain the adsorption behavior of trace metals on the solids. However, the selective chemical precipitation process developed by Zhang and Honaker (2020, 2018) that have

98 proven to be effective for concentrating REEs from AMD has some unique characteristics, such as (1)
99 more complex mineral compositions relative to the synthetic minerals, and (2) shorter residence time
100 relative to the formation of precipitates in the natural environment, as well as in the passive
101 remediation system. Moreover, in some cases, oxidizing agents, such as hydrogen peroxide are
102 required to assist in the removal of iron. Therefore, given the uniqueness of the selective chemical
103 precipitation process, the partitioning behavior and mechanisms obtained in previous studies are not
104 necessarily applicable to the selective chemical precipitation process.

105 In this study, the partitioning behavior of REEs during the chemical precipitation of an AMD was first
106 investigated in the presence and absence of an oxidizing agent. To provide comprehensive insights,
107 precipitation tests were then performed on synthetic AMD solutions comprised of the major
108 constituents in proportions and concentrations found in the actual AMD. Moreover, solution
109 equilibrium calculations, electro-kinetic tests, mineralogy characterization, specific surface area
110 measurements, particle size analysis, and morphology analysis were conducted to identify the
111 mechanisms underlying the partitioning behavior. Understanding the REE partitioning behavior and
112 mechanisms during the precipitation process provides a foundation for separating REEs from major
113 contaminant metal ions when recovering REEs from AMD.

114 ## 2. Material and Methods

115 ### 2.1 Material

116 An AMD sample of around 400 L was collected from a coal preparation plant that treated run-of-
117 mine bituminous coal from the West Kentucky No. 13 (Baker) seam located in western Kentucky,
118 USA. The AMD was generated from a coarse refuse pile due to the oxidation of pyrite under the
119 function of the natural environment. Immediately upon receiving the sample, the AMD was filtered
120 using 5 μm pore size filter paper to remove particulate matter, and the filtrate was uniformly split into
121 19-L buckets, which were tightly sealed to decelerate oxidation. For each precipitation test, a
122 predetermined volume of the AMD was collected from the buckets. Eh and pH of the AMD were first
123 measured to monitor the degree of oxidation of the AMD. Based on the measurement results, it was
124 confirmed that oxidation of the AMD during the overall period of this study was negligible. Moreover,

to obtain a fundamental understanding of the partitioning behavior of REEs during the precipitation, synthetic AMD solutions with major constituents similar to the AMD sample were prepared and used as feeds for precipitation tests.

Sodium hydroxide (NaOH, ⩾97.0 wt. %) was utilized as a pH regulator. Hydrogen peroxide (H_2O_2, 30 wt.%, certified ACS grade) was used as an oxidizing agent to oxidize ferrous to ferric ions. Sodium sulfate (Na_2SO_4, 99.0 wt.%), aluminum chloride hexahydrate ($AlCl_3 \cdot 6H_2O$, ⩾98.0 wt.% purity), and iron (II) chloride tetrahydrate ($FeCl_2 \cdot 4H_2O$, ⩾99.0 wt.%) were utilized to prepare synthetic solutions. All the chemicals were purchased from Thermo Fisher Scientific, USA. A rare earth calibration standard for ICP analysis (High-Purity Standards, LLC, USA), containing 100 ppm of each REE in 5% HNO_3, was used as a source of REEs when preparing the synthetic AMD solutions. All solutions were prepared with Type I deionized water with a resistivity of 18.2 MΩ·cm at 25 °C.

2.2 Methods

2.2.1 Precipitation Test

Precipitation tests were performed on both the natural AMD and the synthetic AMD solutions to investigate the partitioning behavior of REEs. The tests were performed in a glass beaker of 1 L maximum volumetric capacity at room temperature. For each experiment, 0.5 L of the liquid samples were added to the beaker. During the test, the system was continuously stirred using a magnetic stirrer at 500 rpm. Small incremental pH increases were achieved by adding 0.2 mL of 5 mol/L NaOH solution. After each addition, the system was mixed for 2 min to eliminate non-selective precipitation caused by localized concentrations of the base solution. The pH values at the end of each mixing were recorded. Bulk precipitates were generated with increases in the solution pH. Representative samples of 5 mL were collected from the beaker when the pH reached certain values, such as 3.0, 4.0, 5.0, 6.0, 7.0, 8.0, 9.0, 10.0, 11.0, and 12.0. Immediately upon collection, the samples were subjected to solid-liquid separation through centrifuging at 4000 rpm for 10 min. Resultant supernatants were collected

for elemental analysis using inductively coupled plasma mass spectrometry (ICP-MS; Thermo Electron X-Series, Thermo Fisher Scientific, USA). The precipitation removal of REEs and other metal ions was calculated based on elemental concentrations of the feed and supernatants, while the dilution effect caused by the incremental NaOH additions and representative sample collections was also considered in the calculations.

2.2.2 Precipitate Characterization

Selected precipitates generated from the precipitation of the synthetic solutions were subjected to different types of characterizations to reveal the partitioning mechanisms of the REEs. To obtain enough precipitates for characterization, the pH of the synthetic solutions (0.5 L) was increased to a predetermined value following the same procedure described in section 2.2.1, but without collecting representative samples during the pH rise. After being collected through centrifuging, the precipitates were freeze-dried at –54 °C using a Labconco Freezone 4.5 Liter Freeze Dryer (Labconco, Kansas City, KS, USA). The mineralogy of the precipitates was investigated through X-ray diffraction (XRD) analysis, which was carried out using a Bruker D8 Advance Twin diffractometer along with a Cu X-ray source (Bruker Corporation, USA). The operating voltage and current of the X-ray tube were 40 kV and 40 mA, respectively. Scans were conducted at room temperature from 10° to 70° with a step size of 0.02° 2θ and a step time of 0.05 s. Scanning data was recorded digitally, and peak positions, intensities, and corresponding mineral phases were identified using MDI Jade 6 software.

Brunauer-Emmett-Teller (BET) specific surface area (SSA) of the precipitates was measured using a surface area and pore size analyzer (Autosorb-1 Series, Quantachrome, USA). The measurements were conducted under nitrogen atmosphere (adsorption-desorption isotherms at 77 K) in a volumetric working device. The moisture contained in the samples was first removed by drying at 25 °C for 18 h prior to the analysis. The measurements were repeated three times for each sample. Based on the BET theory, the adsorption isotherm was used to determine the SSA through the following equation:

$$SSA_{BET} = \frac{N_A V_m A_n}{V_0} \quad \text{Eq. (5)}$$

where N_A is the Avogadro constant, V_m the amount of gas needed to cover the surface with a monolayer, V_0 the molar volume of gas, and A_n the surface area occupied by a single adsorbed gas molecule. For nitrogen, A_n is usually assumed as 16.21×10^{-20} m^2 (Barbara Lothenbach, Karen Scrivener, 2018).

To further investigate the particle size and morphology of the precipitates, scanning electron microscopy (SEM) analysis was performed using a JSM-IT500HR SEM (JEOL, Peabody, MA, USA) equipped with an Ultim Max EDS detector (Oxford Instruments, Abingdon, UK). A representative portion of the precipitates needed to be characterized were sprinkled onto double-sided carbon tape mounted on an SEM stub. A layer of Au/Pd of 5 nm thickness was coated onto the specimens using a Cressington 208HR Sputter (Cressington Scientific Instruments, UK) to improve their conductivity.

Electro-kinetic tests were performed to measure the zeta potential values of the precipitates during the precipitation process of the synthetic AMD solutions. The same experimental procedures as the precipitation of the natural AMD were employed. Samples were collected during the precipitation process at predetermined pH values and transferred to a capillary cell for zeta potential measurement, which was conducted using a Zs90 Zeta spectrometer (Nano series, Malvern Instruments, UK). Three duplicates were performed for the same solution. Average zeta potential values are reported, and experimental errors are presented as error bars in the figures.

Solution equilibrium calculations were conducted to simulate the precipitation pH of REEs from the natural AMD and to investigate the speciation of metal ions in the synthetic AMD. All the calculations were performed using Visual MINTEQ 3.1 software, which is a freeware chemical equilibrium model maintained by Jon Petter Gustafsson at KTH, Sweden, since 2000. For all the calculations, temperature was fixed at 25 °C.

3. Results and Discussion

3.1 Sample Characterization

The natural AMD used in this study contained 6.6 ppm of total REEs (TREEs), which is relatively high compared to other AMD sources reported in the literature (Honaker et al., 2018; Stewart et al., 2017; Vaziri Hassas et al., 2020; Zhao et al., 2007). In 2011, the U.S. Department of Energy identified Nd, Eu, Tb, Dy, and Y as critical rare earths (Chu, 2011). As shown in Table 1, Y, Nd, and Dy accounted for 20.5%, 16.6%, and 4.2% of the TREEs, respectively. Therefore, more than 40% of the TREEs existing in the AMD are critical REEs. Moreover, the AMD also contained 58 ppm of Mn, 1.65 ppm of Co, and 1.39 ppm of Li, all of which have been identified as critical elements by the US Department of the Interior (Petty, 2018). Given these facts, this AMD may have the potential to be a promising source for the recovery of REEs and other critical elements.

Table 1. Elemental concentration (ppm) of the AMD sample.

Element	*Sc*	*Y*	*La*	*Ce*	*Pr*	*Nd*	*Sm*	*Eu*	*Gd*	*Tb*	*Dy*	*Ho*
Concentration	0.13	1.35	0.79	1.67	0.25	1.09	0.29	0.07	0.36	0.05	0.27	0.05
% of TREEs	2.0	20.5	12.0	25.4	3.70	16.6	4.5	1.0	5.4	0.7	4.2	0.7
Element	*Er*	*Tm*	*Yb*	*Lu*	*LREEs*		*HREEs*		*TREEs*		*HREEs/LREEs*	
Concentration	0.12	0.01	0.08	0.01	4.23		2.36		6.60		0.56	
% of TREEs	1.8	0.2	1.2	0.2	64.2		35.8		100		-	
Element	*Co*	*Cu*	*Ni*	*Zn*	*Li*	*Mn*	*Fe*	*Al*	*Ca*	*Mg*	*Sulfate*	*pH*
Concentration	1.65	2.42	4.73	7.63	1.39	58	884	350	417	302	7,000	2.70

Note: LREEs represents light REEs, including La, Ce, Pr, Nd, Sm, and Sc; HREEs represents heavy REEs, including Eu, Gd, Tb, Dy, Ho, Er, Tm, Yb, Lu, and Y.

3.2 REE Partitioning Behavior during the Precipitation of the Natural AMD

Removal of major, rare earth, and other valuable elements from the natural AMD as a function of pH are shown in Figure 2. Additionally, experimental errors measured by repeating the tests three times are provided in the supplementary document (Table S1 and Table S2). As the solution pH was increased, Fe precipitated first with 23% being removed from the AMD at pH 4.0. It can be observed from the trend of the iron precipitation curve that the rate of Fe removal reduced as the pH continued to increase to 6.0. The rapid precipitation of Fe was restored when the pH was above 6.0. Prior studies

have shown that ferric ions completely precipitate at pH values less than 4.0 (Zhang and Honaker, 2020, 2018). However, only 23% of Fe was precipitated from the AMD at pH 4.0. Therefore, ferric and ferrous ions co-existed in the AMD. Relative to Fe, Al started precipitation at a higher pH value of 4.0. After the pH was increased to around 5.0, nearly 100% of the Al was precipitated. Similarly, TREEs also started to segregate from the solution at around pH 4.0. In contrast to Al, a pH increase to 5.0 only led to 25% removal of the TREEs. Nearly 100% removal of TREEs was achieved at a pH value of around 7.0. Other valuable metals, including Zn, Ni, Co, and Mn, were removed in the pH range of around 5.0-9.0. Alkaline earth metal ions, primarily Ca^{2+} and Mg^{2+}, were the dominant species remaining in the solution when the pH was above 9.0.

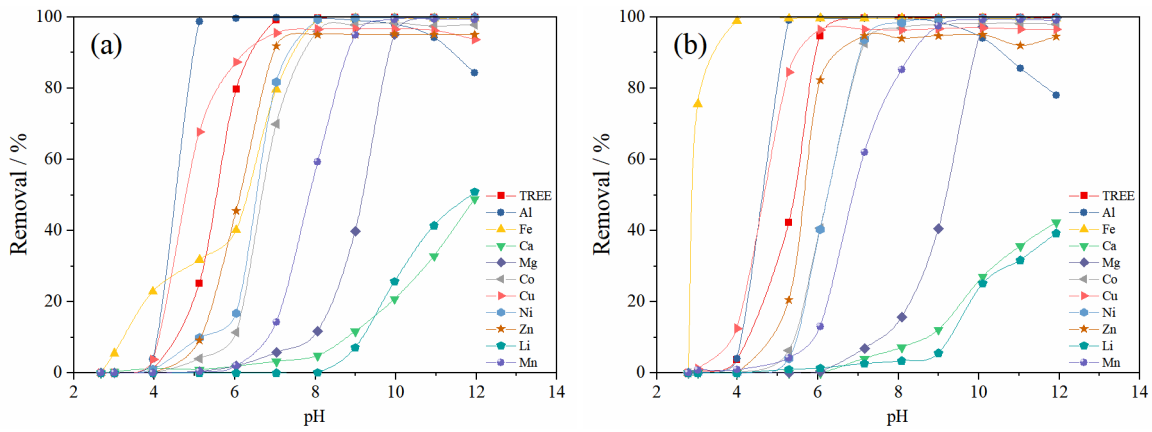

Figure 2. Removal of the major, rare earth, and other valuable elements from the natural AMD using 5 M NaOH (a) without and (b) with the addition of H_2O_2.

Under the function of oxygen and bacteria in the natural environment, oxidation of ferrous to ferric ions existing in AMD readily occurs (Jönsson et al., 2005). Therefore, H_2O_2 was added into the AMD prior to the precipitation test to convert ferrous to ferric ions. Based on Eq.(6), the stoichiometric ratio between Fe^{2+} and H_2O_2 is 2:1. For 884 ppm (1.58×10^{-2} M) of iron in 0.5 L AMD, 7.95×10^{-3} M hydrogen peroxide was needed to oxidize the iron. However, 0.5 vol.% (4.90×10^{-2} M) H_2O_2 was added to ensure the Fe^{2+} was completely oxidized. As shown in Figure 2(b), nearly 80% of Fe was precipitated at pH 3.0, and, as the pH increased to 4.0, Fe was completely precipitated. As

shown in Figure 3, the removal of all individual REEs from the AMD without the addition of H_2O_2 gradually increased as the solution pH increased within the range of 4.0 to 7.0. HREEs were removed from the AMD at lower pH values as compared with LREEs. For example, 50% of Lu was lost at around pH 4.9 while La required a pH value of 6.0 to achieve the same loss. Direct comparisons of the pH corresponding to 10%, 25%, 50%, 75%, and 90% removal of the individual REEs are presented in TableS3, which also confirm this conclusion. Despite being included in LREEs, Sc is the most readily removed among all the REEs. As shown, 50% of the Sc was removed at around pH 4.6, under which condition, the removal of other REEs was less than 30%. This could be due to the ionic radius of Sc^{3+} being smaller than other rare earth elements, and as such, with the same charge as the other REE^{3+}, Sc^{3+} has a higher tendency to hydrolysis than the other REE^{3+}.

$$2Fe^{2+} + H_2O_2 + 2H^+ \rightarrow 2Fe^{3+} + 2H_2O \qquad \text{Eq. (6)}$$

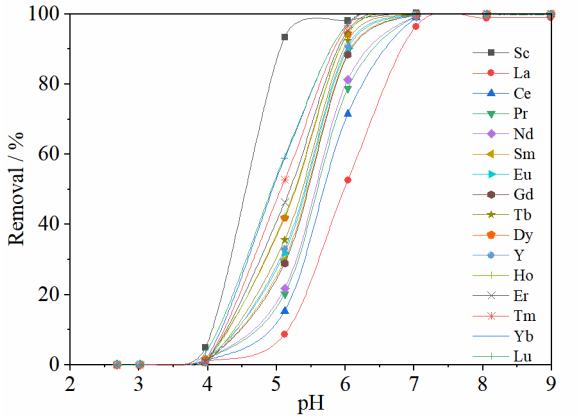

Figure 3. Precipitation removal of individual REEs from the AMD without the addition of H_2O_2.

To predict the precipitation pH of the REEs in the AMD, solution equilibrium calculations were conducted using Visual MINTEQ 3.1 software. The compositions and concentrations shown in Table 1 were used as input. The precipitation pH of REEs were predicted based on saturation indices (SI):

$$SI = log\frac{IAP}{K_{sp}} \quad \text{Eq. (7)}$$

where IAP and K_{sp} represent ion-activity product and solubility product constant, respectively. When $SI > 0$, the solution is oversaturated and precipitation will occur; when $SI < 0$, the solution is under-saturated, and precipitation will not occur; and when $SI = 0$, there is an apparent equilibrium with respect to the solid. Per the calculation results shown in Table 2, it can be concluded that none of the REEs are expected to precipitate at pH values less than 7.0. Therefore, during the precipitation tests, the REEs were removed more likely through adsorption on the surface of the precipitates of the dominant species, such as Al and Fe, rather than precipitation by themselves. This conclusion agrees with the findings from prior studies (Lozano et al., 2020, 2019; Verplanck et al., 2004; Zhang and Honaker, 2018).

Table 2. Precipitation pH of the REEs predicted through solution equilibrium calculations.

Precipitate	$ScOOH_{(s)}$	$La(OH)_{3(s)}$	$Ce(OH)_{3(s)}$	$Pr(OH)_{3(s)}$	$Nd(OH)_{3(s)}$
Case I[a]	np[c]	9.28	9.02	9.15	8.48
Case II[b]	np	9.30	9.04	9.17	8.51
Precipitate	$Sm(OH)_{3(s)}$	$Eu(OH)_{3(s)}$	$Gd(OH)_{3(s)}$	$Tb(OH)_{3(s)}$	$Dy(OH)_{3(s)}$
Case I	8.11	8.06	7.66	8.14	8.00
Case II	8.14	8.08	7.69	8.16	8.02
Precipitate	$Y(OH)_{3(s)}$	$Ho(OH)_{3(s)}$	$Er(OH)_{3(s)}$	$Yb(OH)_{3(s)}$	$Lu(OH)_{3(s)}$
Case I	8.16	8.12	7.91	7.99	8.16
Case II	8.19	8.14	7.93	8.01	8.18

Note: [a] All the iron occurred as ferrous ions; [b] All the iron occurred as ferric ions; [c] No precipitate (np) was formed.

The effect of H_2O_2 addition on the removal of TREEs, LREEs, HREEs, and Sc, as well as individual REEs are presented in Figure 4 and Figure S1, respectively. As shown, the addition of H_2O_2 shifted the partitioning curves of both LREEs and HREEs to lower pH values. In the pH range of 4.0 to 7.0, the removal of REEs at the same pH was noticeably improved. For example, at around pH 5.0, the removal of LREEs and HREEs increased from around 18% and 32% to around 30% and

283 43%, respectively. In contrast with the other REEs, the partitioning curves of Sc obtained with and
284 without the addition of H_2O_2 nearly overlapped, suggesting that the impact of H_2O_2 addition on the
285 removal of Sc was minimal. Given these findings, it can be concluded that the formation of ferric
286 precipitates in the AMD contributed to the removal of the REEs, with Sc being the exception. The
287 except may be due to the smaller ionic radius while higher hydrolysis tendency of Sc^{3+} relative to the
288 other REE^{3+}.

289 Based on the precipitation characteristics of the major and rare earth elements, the majority of Fe
290 and Al can be removed from the AMD by adding H_2O_2, increasing the pH to 5.0, and separating the
291 generated precipitates by solid-liquid separation. Afterward, a concentrate of REEs can be obtained by
292 collecting the precipitates that are formed as the pH of the liquid increases to higher values (e.g., 8.5).
293 However, the negative effect is that a portion of the REEs will be lost to the precipitates of Fe and Al.
294 Therefore, it is essential to assess the partitioning behavior and mechanisms of REEs during the
295 precipitation process for the concentration of REEs from AMD.

296 The major conclusions drawn in this section regarding the partitioning behavior of REEs in the
297 precipitation of actual AMD are summarized as follows: (1) the conversion of ferrous to ferric ions
298 increased the removal of REEs from the AMD; and (2) the REEs were removed by adsorption other
299 than precipitation by themselves. REE partitioning behavior during the precipitation of synthetic
300 AMD was evaluated to confirm the conclusions.

301

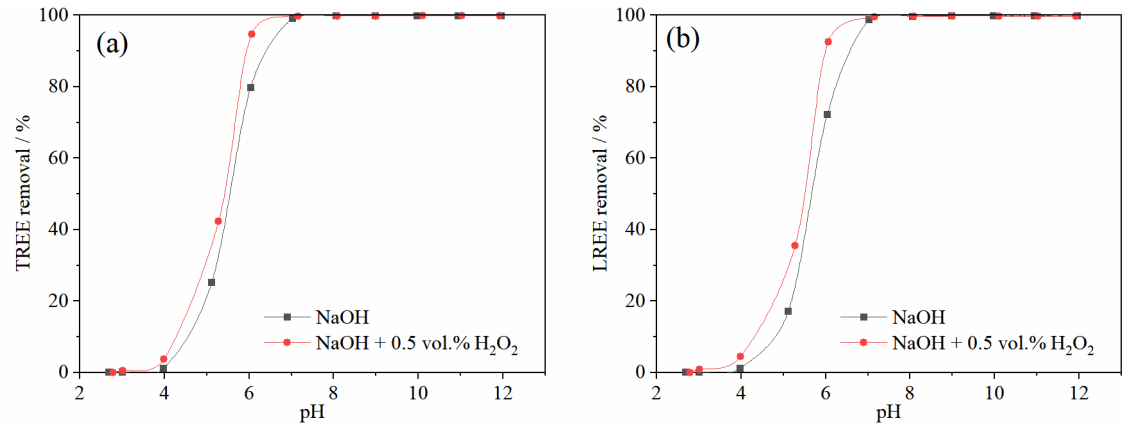

302

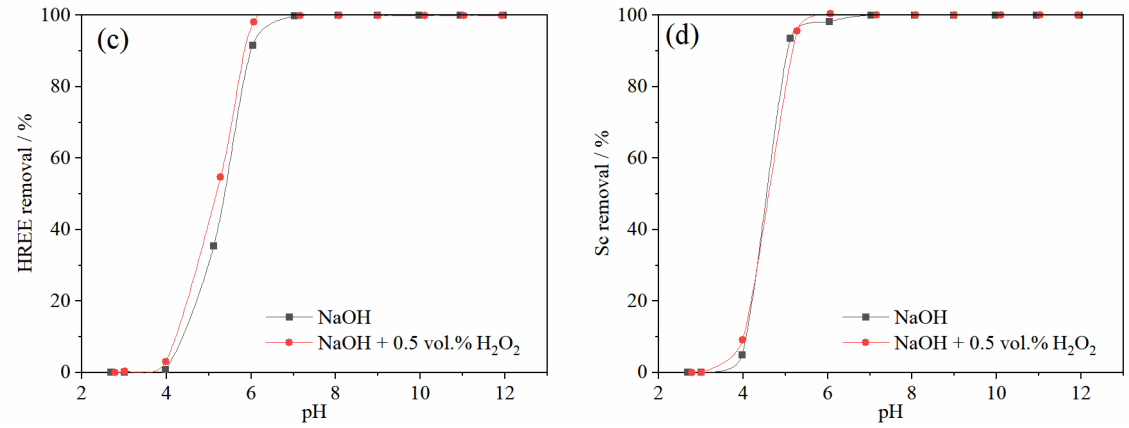

Figure 4. Effects of H_2O_2 addition on the precipitation removal of (a) TREEs, (b) LREEs, (c) HREEs, and (d) Sc.

3.3 REE Partitioning Behavior during the Precipitation of Synthetic AMD

To obtain in-depth insights about the partitioning behavior of REEs during the precipitation of AMD, precipitation tests were performed on synthetic AMD solutions with major constituents similar to the natural AMD investigated in the current study. Moreover, as presented in Figure 2, the conversion of ferrous to ferric ions affected the partitioning behavior of REEs. Therefore, with the total concentration of iron being fixed, H_2O_2 was added to selected synthetic solutions to alternate the valence state of iron. Four synthetic solutions referred to as Solution I, II, III, and IV were prepared and subjected to precipitation tests. The primary elemental compositions of the four solutions are presented in Table 3.

Table 3. Primary elemental compositions of the four synthetic solutions.

Solution	Al^{3+}	Fe^{2+}	SO_4^{2-}	Each REE	H_2O_2
	ppm	ppm	ppm	ppm	vol./%
Solution I	400	900	7000	1	/
Solution II	400	900	7000	1	0.5
Solution III	400	/	7000	1	/

Solution IV	/	900	7000	1	0.5

318

319 As shown in Figure 5(a), Fe was barely removed from Solution I at pH 4.0 whereas, at the same
320 pH, removals close to 100% were obtained from Solution II and IV. The contrast suggested that the
321 addition of 0.5 vol.% H_2O_2 completely oxidized Fe^{2+} to Fe^{3+}. The removal curves of Al^{3+} in Solution I,
322 II, and III almost overlapped, with nearly 100% being removed at pH 5.0 (Figure 5(b)). This
323 phenomenon aligned with the observations obtained from the natural AMD (Figure 2). Slight
324 differences in Al removal from the three solutions were observed at pH 4.0. As shown, the removal
325 from Solution I and III at this pH equated to zero, whereas around 7.4% of Al was removed from
326 Solution II. Therefore, it can be concluded that the precipitation of Fe^{3+} at pH values below 4.0
327 contributed to the removal of Al^{3+}.

328 The removals of TREEs, LREEs, HREEs, and Sc as a function of pH are presented in Figures
329 5(c)-(f), respectively, while those of other individual REEs are provided in the supplementary
330 document. A comparison between REE removals from Solution I and II suggested that the conversion
331 of ferrous to ferric ions contributed to the removal of REEs. This phenomenon agreed with the
332 findings observed from the AMD (Figure 2), which can be explained by the conclusion drawn from
333 the following experimental data that ferric precipitates have higher adsorption capability toward REEs
334 relative to aluminum precipitates. As shown in Figure 5(c), 50% of TREEs were removed from
335 Solution IV at around pH 4.32, whereas a pH value of around 5.38 was needed to achieve the same
336 removal from Solution III. However, an opposite result was obtained in the research conducted by
337 Ayora et al. (2016) that schwertmannite does not accumulate rare earth elements, which, instead, are
338 retained in the basaluminite residue.

339 A column setup filled with calcite and wood shavings was used in the study by Ayora et al.
340 (2016), and AMD was allowed to flow through the column. The process was continued up to 30
341 weeks, after which Fe^{3+}-rich precipitate and Al^{3+}-rich precipitate were collected separately. The
342 partitioning behavior of REEs was evaluated based on elemental compositions of the precipitates.

343 Based on the description, it can be concluded that in the study by Ayora et al. (2016), Fe^{3+} and Al^{3+}
344 were simultaneously precipitated, and then the Fe^{3+} and Al^{3+} precipitates were segregated in the
345 column under the function of density difference. However, in the present study, the precipitation tests
346 were conducted in beakers with continuous stirring, and as such, the iron and aluminum in the
347 synthetic AMD sequentially precipitated with gradual increases in pH. These contrasts may lead to the
348 opposite conclusions.

349 As aforementioned, after adding 0.5 vol.% H_2O_2, the major metal ions in Solution II were 400
350 ppm Al^{3+} and 900 ppm Fe^{3+}, while for Solution IV, the dominant metal ions were 900 ppm Fe^{3+}.
351 Therefore, in the pH range of 4.0-7.0, the amount of precipitate formed in Solution II was larger than
352 in Solution IV, since both ferric and portions of aluminum precipitated from Solution II. With more
353 adsorbent, REE removal from Solution II was expected to be larger than that from Solution IV.
354 However, Figure 5(c)-(f) show that much higher removals of REEs were obtained from Solution IV
355 relative to Solution II. Therefore, the removal of REEs was controlled by factors other than the
356 amount of precipitates existing in the solution alone.

357 More specific comparisons among the four solutions were conducted by evaluating the recoveries
358 at pH 4.0. In Solution I and III, both Al and Fe were not precipitated; thus, REE removals equated to
359 zero since there is no adsorbent in the system. In Solution II, nearly 100% of Fe was precipitated,
360 leading to a TREE removal of around 8%. However, with nearly the same amount of Fe being
361 precipitated, much higher removal of around 37% was obtained from Solution IV. The only difference
362 between the two solutions in terms of elemental composition is that Solution II contained 400 ppm of
363 Al in addition to 900 ppm of Fe. Moreover, as aforementioned, around 7.4% of Al was removed at pH
364 4.0 from Solution II due to the Fe^{3+} precipitates. Therefore, it can be concluded that the presence of
365 aluminum species reduced the removal of REEs from Solution II.

366 Solution I contained 900 ppm of Fe in addition to 400 ppm of Al, while Solution III only
367 contained 400 ppm of Al. As shown in Figure 5(a) and (b), the precipitation removals of Al from the
368 two solutions were similar, whereas certain portions of Fe were removed from Solution I in the pH
369 range of 4.0-6.0. Larger removals of REEs were expected from Solution I relative to Solution III since

more precipitates existed in Solution I, which provided more active sites for REE adsorption. However, as shown in Figure 5(c) to (f), as pH increased from 4.0 to 6.0, the removal of REEs from Solution I was first lower and then higher than Solution III. Therefore, it can be concluded that the presence of ferrous ions influenced the removal of REEs from Solution I.

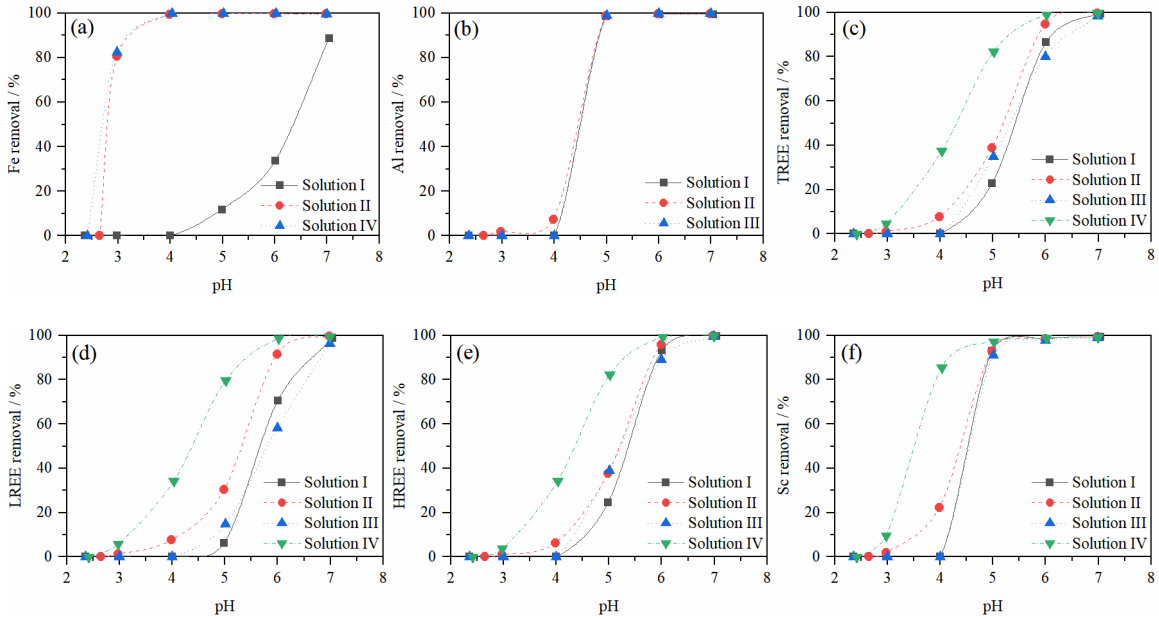

Figure 5. Precipitation removal of (a) Fe, (b) Al, (c) TREE, (d) LREE, (e) HREE, and (f) Sc from the synthetic solutions.

Compared with other REEs, Sc was more likely adsorbed onto the surface of Al and Fe precipitates. As shown in Figure 5(f), nearly 85% of Sc was removed at pH 4.0 from Solution IV, and regardless of the interaction between Al and REEs, a much higher removal of around 22% relative to the other REEs was obtained from Solution II at the same pH value. Moreover, Solution I and III had nearly the same Sc removals within the investigated pH range, which indicated that ferrous ions had no effect on the Sc removal. This phenomenon may be due to the stronger adsorption capacity of Sc on the precipitate surfaces. Compared with the test results of the natural AMD shown in Figure 3(d), larger removal increases at pH 4.0 caused by adding H_2O_2 were achieved for the synthetic solutions (Solution II versus Solution I). The contrast suggested that, in addition to the aluminum and iron

389 species and precipitates, other solution components in the natural AMD also influenced the
390 partitioning behavior of Sc.

391 The major conclusions drawn in this section regarding the partitioning behavior of REEs in the
392 precipitation of synthetic AMD are summarized as follows: (1) the precipitation of Fe^{3+} contributed to
393 the removal of Al^{3+}; (2) the ferric precipitates showed higher removal capacity toward REEs than the
394 aluminum precipitates; (3) the conversion of ferrous to ferric ions increased the removal of REEs
395 from the synthetic AMD, while the increase was reduced in the presence of Al^{3+}; and (4) in the
396 synthetic solutions comprised of Al^{3+} and Fe^{2+}, the precipitation of Al^{3+} contributed to the removal of
397 REEs, while the removal was affected by the Fe^{2+}. These conclusions are consistent with those drawn
398 in section 3.3.

399

400 **3.4 Characterization of the Precipitates Obtained from the Synthetic AMD**

401 Precipitation test results of both the natural and synthetic AMD solutions presented in the
402 previous section suggested that the partitioning of REEs during the precipitation process was
403 primarily due to adsorption on the surface of the dominant precipitates. Moreover, the dominant
404 species existing in the solutions, such as Al^{3+}, Fe^{3+}, and Fe^{2+}, largely affected the adsorption of the
405 REEs. Since adsorption behavior is sensitive to solid surface characteristics, selected precipitates
406 formed from the synthetic solutions were characterized in terms of mineralogy, surface zeta potential,
407 specific surface area, particle size, and morphology.

408 **3.4.1 Mineralogy Characterization**

409 The crystallinity of iron and aluminum precipitates formed in the acidic, sulfate-rich environment
410 has been studied in previous research (Carrero et al., 2017; Regenspurg et al., 2004). Poorly
411 crystallized iron hydroxysulfate and aluminum hydroxysulfate minerals, such as schwertmannite and
412 basaluminite, were found by XRD analysis (Bigham et al., 1994; Bao et al., 2018; R. Richmond et al.,
413 2004). However, as shown in Figure 6, the X-ray diffractograms of the precipitates formed from the
414 synthetic solutions are dispersed and mineral phases were not found by analyzing with MDI JADE 6.0

software. This contrast is likely due to the fact that the crystallization of precipitates is largely determined by aging time. A longer aging time normally results in a higher crystallinity, however, in the current study, the precipitates were filtered immediately after precipitation without aging. The absence of aging likely explains the amorphous characteristic of the precipitates (Jiménez et al., 2019).

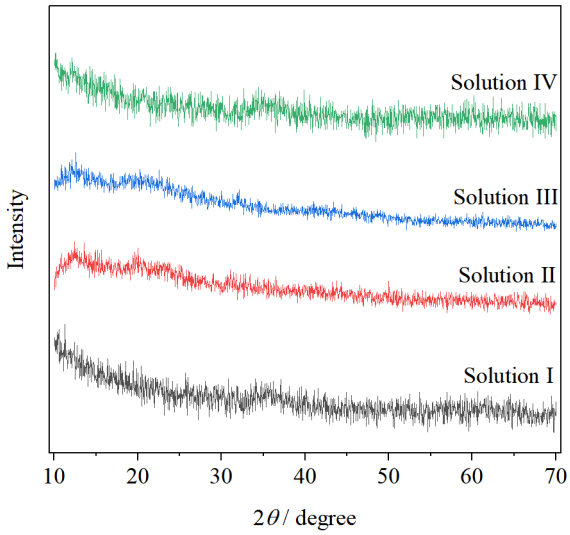

Figure 6. X-ray diffractograms of the precipitates obtained from Solution I, II, III, and IV at pH 5.

3.4.2 Electro-kinetic Tests

Since the surface charge of the precipitates can significantly influence the adsorption of REEs on the precipitates, electro-kinetic tests were performed on the precipitates formed in the synthetic solutions. In the pH range of 3.0 to 8.0, the iron precipitates obtained from Solution IV had the highest negative zeta potential values as compared to the precipitates formed in Solution I, II, and III, which may enhance the adsorption of positively charged REE species (Figure 7). This observation aligns with the fact that the removal of REEs in Solution IV was much higher than that in the other synthetic solutions (Figure 5(c-f)). This evidence supports the hypothesis that electrostatic interactions play an essential role in the removal of REEs during the precipitation process.

In the pH range of 3.0 to 4.0, iron was completely precipitated for both Solution II and IV (Figure 5(a)); however, the negative charges of the precipitates formed in Solution II were much lower than

433 those of the precipitates formed in Solution IV. This phenomenon could be due to the presence of Al
434 in Solution II, which may have adsorbed on the precipitates and neutralized the negative charge of the
435 precipitates. Solution equilibrium calculations showed that, at pH 3.5, $AlSO_4^+$ is the only positively
436 charged species accounting for a considerable portion of total Al (Table 4). As such, the decreases in
437 the negative zeta potential values of the ferric precipitates were likely caused by the adsorption of
438 $AlSO_4^+$. It is postulated that the reduced negative charges impaired the electrostatic attractions
439 between REEs and the ferric precipitates, and as a result, the removals of REEs from Solution II were
440 lower than those from Solution IV. Moreover, the Al species in Solution II might also compete with
441 the REE species for the active sites on the iron precipitates during the precipitation process. Therefore,
442 it can be concluded that the presence of Al in AMD reduces the removal of REEs during the
443 precipitation process. In other words, the loss of REEs with the precipitates of the major contaminant
444 metal ions was decreased in the presence of aluminum.

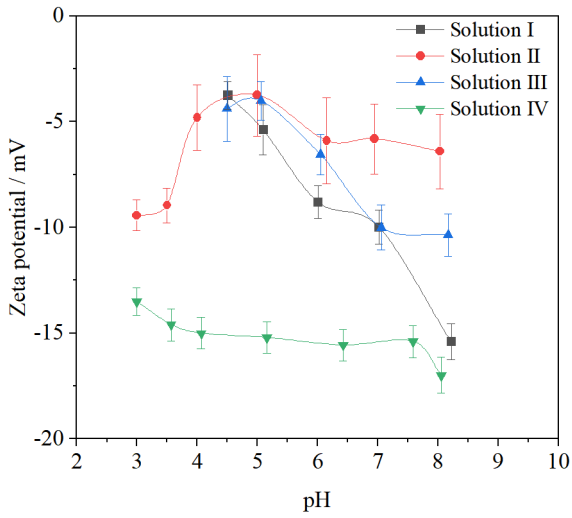

445

446 **Figure 7**. Zeta potential of the precipitates obtained from Solution I, II, III, and IV as a function of pH
447 values.

448 **Table 4.** Species distributions (%) of the following solutions: (1) 400 ppm Al^{3+} in a solution containing
449 7000 ppm SO_4^{2-} at pH 3.5 and (2) 900 ppm Fe^{2+} containing 7000 ppm SO_4^{2-} at pH 4.5.

Species	Al^{3+}	$AlSO_4^+$	$Al(SO_4)_2^-$	$Al(OH)^{2+}$	Total

Distribution	2.94	48.39	48.65	0.03	100

Species	Fe^{2+}	$FeSO_{4(aq)}$	Total
Distribution	36.67	63.33	100

As Table 4 shows, solution equilibrium calculations indicated that $FeSO_{4(aq)}$ was the dominant active species in Solution I in the pH range of 4.0-5.0. Since this species does not carry charges, rather than electrostatic attraction, the species was more likely adsorbed onto the aluminum precipitate surface and competed with the REE species through specific interactions, such as hydrogen bonding. This conclusion can be corroborated by the fact that in the pH range of 4.0-5.0, the zeta potential values of Solution I were close to those of Solution III. Due to the specific interactions, REE removals from Solution I were lower than Solution III in the pH range of 4.0-5.0 (see Figure 5(c)-(e)). As pH continued to increase above 5.0, the negative zeta potential values of the precipitates formed in Solution I were largely increased, and at pH 8.0, the precipitates formed in Solution I and IV have similar zeta potential. Since Solution IV only contained ferric precipitates, it can be concluded that at pH above 5.0, rather than adsorption on the aluminum precipitate surface, the precipitation of ferrous ions themselves occurred, and the new precipitates have similar characteristics as the ferric precipitates. With the new precipitates being generated in the pH range of 5.0-8.0, more adsorbent was available in Solution I, and the negative impacts of $FeSO_{4(q)}$ on REE adsorption were offset, and ultimately, higher REE removals were obtained relative to Solution III (see Figure 5(c)-(e)).

3.4.3 Specific Surface Area and Morphology Analyses

As another important characteristic of precipitates, specific surface area (SSA) can effectively influence their adsorption efficiency. The SSA of the different precipitates obtained from the synthetic solutions at different pH values is shown in Figure 8. Conditions for preparing the precipitates were the same as those used for the precipitation tests, except that REEs were not added in the feed solutions. The precipitates formed from the Solution II and IV at pH 4 was expected to have similar SSA since nearly 100% of Fe was precipitated at this pH for both solutions (see Figure 5); however,

as shown in Figure 8, the SSA of the precipitates formed from Solution IV was significantly larger than that of the precipitates from Solution II (72.74 m^2/g versus 17.19 m^2/g). As concluded from the electro-kinetic test results, the aluminum species existing in Solution II adsorbed on the surface of the iron precipitates and reduced their negative zeta potential. The reductions in zeta potential values likely promoted the coagulation of the iron precipitate particles, thereby reducing the SAA.

The precipitates obtained from Solution III and IV consisted of only aluminum and iron precipitates, respectively. As shown in Figure 8, the SSA of the aluminum precipitates was larger than that of the iron precipitates (115.63 m^2/g versus 71.57 m^2/g). As pH was raised from 4.0 to 5.0, both iron and aluminum precipitated in Solution II which resulted in increases in the SSA of the precipitates from 17.19 to 60.56 m^2/g. The SSA of the precipitates formed in Solution II (60.56 m^2/g) at pH 5.0 was smaller than that of the precipitates in Solution III (115.63 m^2/g) and Solution IV (71.57 m^2/g). This fact also proved that there were interactions between the Al and Fe species existing in Solution II during the precipitation process; otherwise, the SSA of the precipitates formed in Solution II at pH 5 shall be between that of the precipitates formed in Solution III and Solution IV at the same pH.

Solution I contained 400 ppm of Al^{3+} and 900 ppm of Fe^{2+}; however, the SSA of the precipitates obtained from Solution I at pH 5.0 was only slightly lower than that of the precipitates obtained from Solution III with only 400 ppm of Al^{3+} (111.3 m^2/g versus 115.63 m^2/g). This phenomenon can be explained by the finding from the electro-kinetic tests that ferrous ion adsorption on the aluminum precipitates in Solution I did not largely alter their zeta potential values in the pH range of 4.0 – 5.0 since the active species is neutral ($FeSO_4$). When the pH was elevated from 5.0 to 6.0, the SSA of the precipitates in Solution I increased significantly from 111.3 m^2/g to 184.67 m^2/g. This phenomenon indirectly corroborated the conclusion that precipitation of the ferrous ions in Solution I occurred at pH values above 5.0.

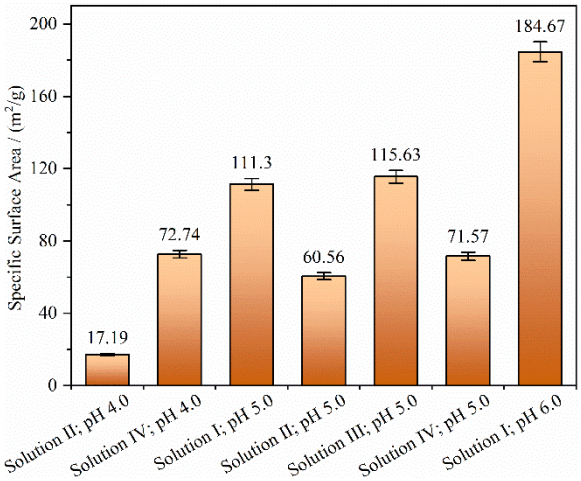

499

500 **Figure 8**. The specific surface area of precipitates from the synthetic solutions at different pH values.

501

502 The morphological features and surface characteristics of the precipitates formed in synthetic
503 AMD solutions were assessed through SEM analysis. As shown in Figure 8, the precipitates obtained
504 from the synthetic solutions were made up of aggregates, which consisted of numerous nanospheres.
505 Comparisons between Figures 9(a) and (b) showed that the nanospheres comprised in the precipitates
506 of Solution II were larger than those in the precipitates of Solution IV. This observation aligned with
507 the finding that, at pH 4, the SSA of the precipitates formed from Solution II were smaller than those
508 from Solution IV (17.19 m^2/g versus 72.74 m^2/g). The findings support the coagulation of ferric
509 precipitates due to the presence of the aluminum species. According to previous research, aluminum
510 salts, such as aluminum sulphate and aluminum chloride, are commonly used as coagulants in the
511 water treatment industry (Lin et al., 2017; Dentel and Gossett, 1988; Wang et al., 2009; He et al.,
512 2019). Comparisons between Figures 9(c) and (d) suggested that the nanospheres comprised in the
513 precipitates of Solution III formed at pH 5.0 were slightly smaller than those comprised in the
514 precipitates of Solution I formed at the same pH. This finding agrees with the fact that the two
515 precipitates from different sources have similar SSA (Figure 8).

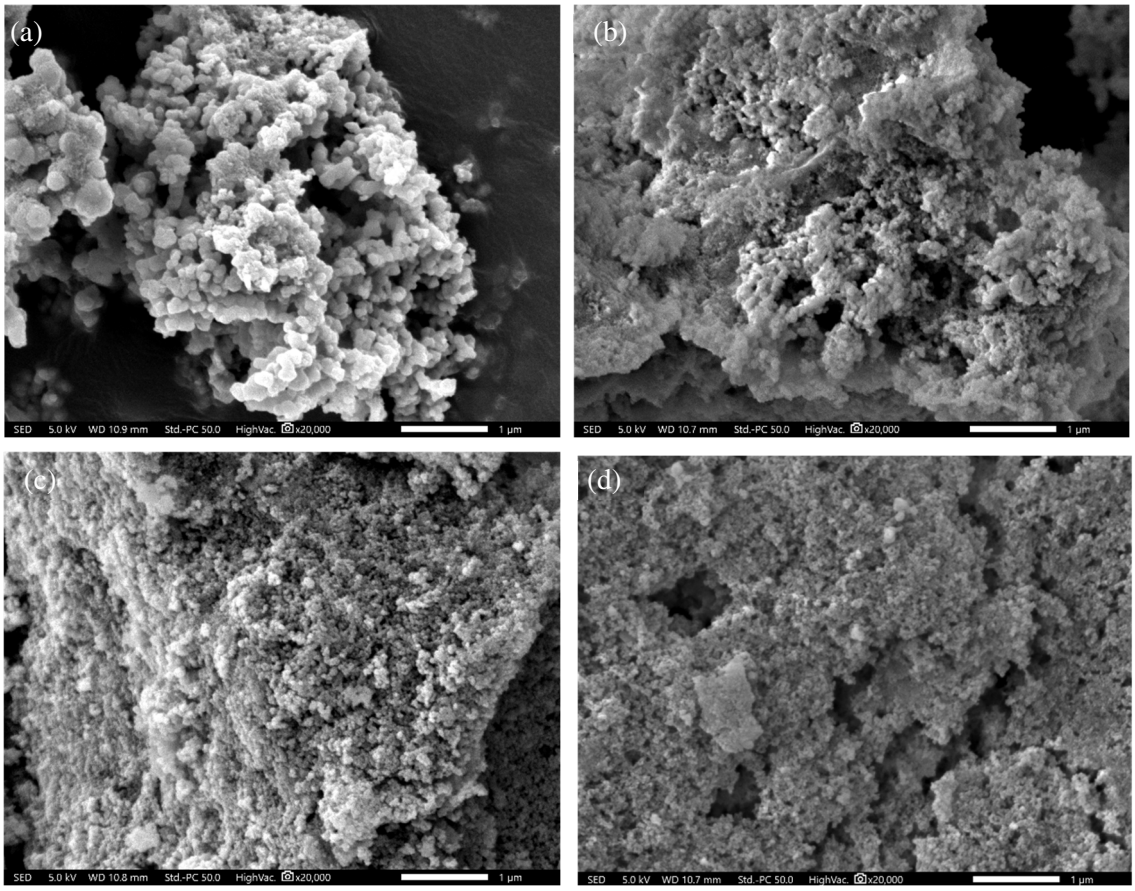

Figure 9. SME images of the precipitate particles obtained from synthetic solutions at different pH values: (a) Solution II pH=4, (b) Solution IV pH=4, (c) Solution I pH=5, and (d) Solution III pH=5.

3.4.4 Summary of the Partitioning Mechanisms and Potential Applications of This Study

Based on the characterizations of the precipitates formed in the synthetic AMD, it was found that ferric precipitates carried more negative charges than aluminum precipitates, thus showing stronger adsorption and removal capacity for REEs. However, in the presence of aluminum ions, the removal of REEs by ferric precipitates was reduced due to the charge neutralization and competitive adsorption effects caused by the aluminum species. In the solutions containing aluminum and ferrous ions, neutral ferrous species ($FeSO_{4(aq)}$) competed with REEs for the active adsorption sites on the aluminum precipitates in the pH range of 4.0-5.0. However, at higher pH, ferrous precipitates were formed, which carried similar negative charges as ferric precipitates, and such, the removal of REEs was improved. In addition, since ferric ions precipitated at lower pH than ferrous ions, the conversion

of ferrous to ferric ions by adding hydrogen peroxide promoted the removal of REEs at lower pH. The findings from this study will contribute to the improvement of the selective chemical precipitation process for REE concentration and recovery from AMD. For example, in the process, Fe and Al are first removed by increasing the pH of AMD to around 4.5-5.0. Based on the findings from this study, it can be concluded that the presence of an appropriate amount of Al in AMD reduces the loss of REEs to the precipitate product. In addition, some chemicals that can compete with REEs for the active adsorption sites on the precipitates can be added to AMD to further reduce the loss of REEs to the precipitate product.

4. Conclusion

An acid mine drainage (AMD) sample was collected from a coal preparation plant that treated run-of-mine bituminous coal from the West Kentucky No. 13 seam. Elemental analyses showed that the sample contained 6.6 ppm of rare earth elements (REEs), which was higher relative to values reported for most AMD sources in the literature. A series of precipitation tests performed on the AMD found that REE removal at pH values below 6.0 were increased by adding H_2O_2. Solution equilibrium calculations suggested that REE removal under these conditions was a result of surface adsorption on the precipitates of the dominant metal ions. The addition of H_2O_2 oxidized ferrous to ferric ions and, as a result, caused the majority of the iron to precipitate at pH values below 4.0. The ferric sulfate precipitates have more active sites for adsorption, which caused adsorption of the positively charged forms of REEs and their subsequent removal as part of the precipitate product.

Precipitation tests were also performed on synthetic AMD solutions containing the major constituents at concentrations similar to the natural AMD sample. Characterization studies on the precipitates provided insights into the REE partitioning behavior and mechanisms during the precipitation process. As compared to the aluminum precipitates formed in the solutions, the iron precipitates had higher adsorption capacity towards REEs, which was found to be primarily due to the fact that more negative charges were carried on the surface of the iron precipitates. Moreover, it was found that the presence of aluminum in an AMD containing ferric ions reduces the REE removal to

557 the precipitate product. This effect was attributed to the decrease in the magnitude of the negative zeta
558 potential values associated with the ferric precipitates caused by aluminum adsorption as well as the
559 competitive adsorption between the aluminum and rare earth species on the active sites of the
560 precipitates. Similarly, the presence of ferrous in an AMD containing aluminum ions also reduces
561 REE loss to the precipitate product. However, at pH values larger than 5.0, REE loss was improved
562 due to the precipitation of ferrous ions, which provided more adsorbent and active sites.

563

564

565 **Acknowledgements**

566 This material is based upon work supported by the U.S. Department of Energy under Award Number
567 DE-FE0031827.

577

578 **References**

579 Achterberg, E.P., Herzl, V.M.C., Braungardt, C.B., Millward, G.E., 2003. Metal behaviour in an
580 estuary polluted by acid mine drainage: The role of particulate matter. Environ. Pollut. 121,
581 283–292. https://doi.org/10.1016/S0269-7491(02)00216-6

582 Alonso, E., M. Sherman, A., J. Wallington, T., P. Everson, M., R. Field, F., Roth, R., E. Kirchain, R.,
583 2012. Evaluating Rare Earth Element Availability: A Case with Revolutionary Demand from
584 Clean Technologies. Environ. Sci. & Technol. 46, 3406–3414.
585 https://doi.org/10.1021/es203518d

586 Ayora, C., Macías, F., Torres, E., Lozano, A., Carrero, S., Nieto, J.-M., Pérez-López, R., Fernández-
587 Martínez, A., Castillo-Michel, H., 2016a. Recovery of Rare Earth Elements and Yttrium from
588 Passive-Remediation Systems of Acid Mine Drainage. Environ. Sci. & Technol. 50, 8255–
589 8262. https://doi.org/10.1021/acs.est.6b02084

590 Ayora, C., Macías, F., Torres, E., Lozano, A., Carrero, S., Nieto, J.M., Pérez-López, R., Fernández-
591 Martínez, A., Castillo-Michel, H., 2016b. Recovery of Rare Earth Elements and Yttrium from
592 Passive-Remediation Systems of Acid Mine Drainage. Environ. Sci. Technol. 50, 8255–8262.
593 https://doi.org/10.1021/acs.est.6b02084

594 Baleeiro, A., Fiol, S., Otero-Fariña, A., Antelo, J., 2018. Surface chemistry of iron oxides formed by
595 neutralization of acidic mine waters: Removal of trace metals. Appl. Geochemistry 89, 129–137.
596 https://doi.org/10.1016/j.apgeochem.2017.12.003

597 Balintova, M., Petrilakova, A., 2011. Study of pH influence on selective precipitation of heavy metals
598 from acid mine drainage. Chem. Eng. Trans. 25, 345–350. https://doi.org/10.3303/CET1125058

599 Bao, Y., Guo, C., Lu, G., Yi, X., Wang, H., Dang, Z., 2018. Role of microbial activity in Fe(III)
600 hydroxysulfate mineral transformations in an acid mine drainage-impacted site from the
601 Dabaoshan Mine. Sci. Total Environ. 616–617, 647–657.
602 https://doi.org/10.1016/j.scitotenv.2017.10.273

603 Barbara Lothenbach, Karen Scrivener, R.S., 2018. A Practical Guide to Microstructural Analysis of
604 Cementitious Materials. CRC Press.

605 Bigham, J.M., Carlson, L., Murad, E., 1994. Schwertmannite, a new iron oxyhydroxysulphate from
606 Pyhäsalmi, Finland, and other localities. Mineral. Mag. 58, 641–648.
607 https://doi.org/10.1180/minmag.1994.058.393.14

608 Carrero, S., Fernandez-Martinez, A., Pérez-López, R., Lee, D., Aquilanti, G., Poulain, A., Lozano, A.,
609 Nieto, J.M., 2017. The nanocrystalline structure of basaluminite, an aluminum hydroxide sulfate
610 from acid mine drainage. Am. Mineral. 102, 2381–2389. https://doi.org/10.2138/am-2017-6059

611 Chu, S., 2011. Critical materials strategy. DIANE Publishing.

612 Dentel, S.K., Gossett, J.M., 1988. Mechanisms of Coagulation With Aluminum Salts. J. / Am. Water
613 Work. Assoc. 80, 187–198. https://doi.org/10.1002/j.1551-8833.1988.tb03025.x

614 Felipe, E.C.B., Batista, K.A., Ladeira, A.C.Q., 2020. Recovery of rare earth elements from acid mine
615 drainage by ion exchange. Environ. Technol. (United Kingdom) 0, 1–32.
616 https://doi.org/10.1080/09593330.2020.1713219

617 Franus, W., Wiatros-Motyka, M.M., Wdowin, M., 2015. Coal fly ash as a resource for rare earth
618 elements. Environ. Sci. Pollut. Res. 22, 9464–9474. https://doi.org/10.1007/s11356-015-4111-9

619 Fukushi, K., Sato, T., Yanase, N., Minato, J., Yamada, H., 2004. Arsenate sorption on schwertmannite.
620 Am. Mineral. 89, 1728–1734. https://doi.org/10.2138/am-2004-11-1219

621 Hassas, B.V., Rezaee, M., Pisupati, S. V., 2021. Effect of various ligands on the selective
622 precipitation of critical and rare earth elements from acid mine drainage. Chemosphere 280,
623 130684. https://doi.org/10.1016/j.chemosphere.2021.130684

624 He, W., Xie, Z., Lu, W., Huang, M., Ma, J., 2019. Comparative analysis on floc growth behaviors
625 during ballasted flocculation by using aluminum sulphate (AS) and polyaluminum chloride
626 (PACl) as coagulants. Sep. Purif. Technol. 213, 176–185.
627 https://doi.org/10.1016/j.seppur.2018.12.043

628 Honaker, R.Q., Zhang, W., Werner, J., Noble, A., Luttrell, G.H., Yoon, R.-H., 2020. Enhancement of
629 a process flowsheet for recovering and concentrating critical materials from bituminous coal
630 sources. Mining, Metall. Explor. 37, 3–20.

631 Honaker, R.Q., Zhang, W., Yang, X., Rezaee, M., 2018. Conception of an integrated flowsheet for
632 rare earth elements recovery from coal coarse refuse. Miner. Eng. 122, 233–240.

633 https://doi.org/10.1016/j.mineng.2018.04.005

634 Huang, S., Zhou, L., 2012. Fe 2+ oxidation rate drastically affect the formation and phase of
635 secondary iron hydroxysulfate mineral occurred in acid mine drainage. Mater. Sci. Eng. C 32,
636 916–921. https://doi.org/10.1016/j.msec.2012.02.012

637 Jiménez, A., Hernández, A., Prieto, M., 2019. Crystallization Behaviour of Iron-Hydroxide Sulphates
638 by Aging under Ambient Temperature Conditions. Minerals 9, 27.
639 https://doi.org/10.3390/min9010027

640 Jönsson, J., Persson, P., Sjöberg, S., Lövgren, L., 2005. Schwertmannite precipitated from acid mine
641 drainage: Phase transformation, sulphate release and surface properties. Appl. Geochemistry 20,
642 179–191. https://doi.org/10.1016/j.apgeochem.2004.04.008

643 Kim, Y., 2015. Mineral phases and mobility of trace metals in white aluminum precipitates found in
644 acid mine drainage. Chemosphere 119, 803–811.
645 https://doi.org/10.1016/j.chemosphere.2014.08.034

646 Lin, J., Couperthwaite, S.J., Millar, G.J., 2017. Effectiveness of aluminium based coagulants for pre-
647 treatment of coal seam water. Sep. Purif. Technol. 177, 207–222.
648 https://doi.org/10.1016/j.seppur.2017.01.010

649 Lozano, A., Ayora, C., Fernández-Martínez, A., 2020. Sorption of rare earth elements on
650 schwertmannite and their mobility in acid mine drainage treatments. Appl. Geochemistry 113.
651 https://doi.org/10.1016/j.apgeochem.2019.104499

652 Lozano, A., Ayora, C., Fernández-Martínez, A., 2019. Sorption of rare earth elements onto
653 basaluminite: The role of sulfate and pH. Geochim. Cosmochim. Acta 258, 50–62.
654 https://doi.org/10.1016/j.gca.2019.05.016

655 MacIngova, E., Luptakova, A., 2012. Recovery of metals from acid mine drainage. Chem. Eng. Trans.
656 28, 109–114. https://doi.org/10.3303/CET1228019

657 Massari, S., Ruberti, M., 2013. Rare earth elements as critical raw materials: Focus on international

markets and future strategies. Resour. Policy 38, 36–43. https://doi.org/10.1016/j.resourpol.2012.07.001

Petty, T.R., 2018. Final List of Critical Minerals 2018. Fed. Regist. 83, 23295–23296.

R. Richmond, W., Loan, M., Morton, J., M. Parkinson, G., 2004. Arsenic Removal from Aqueous Solution via Ferrihydrite Crystallization Control. Environ. Sci. & Technol. 38, 2368–2372. https://doi.org/10.1021/es0353154

Regenspurg, S., Brand, A., Peiffer, S., 2004. Formation and stability of schwertmannite in acidic mining lakes. Geochim. Cosmochim. Acta 68, 1185–1197. https://doi.org/10.1016/j.gca.2003.07.015

Sprecher, B., Kleijn, R., Kramer, G.J., 2014. Recycling potential of neodymium: The case of computer hard disk drives. Environ. Sci. Technol. 48, 9506–9513. https://doi.org/10.1021/es501572z

Stewart, B.W., Capo, R.C., Hedin, B.C., Hedin, R.S., 2017. Rare earth element resources in coal mine drainage and treatment precipitates in the Appalachian Basin, USA. Int. J. Coal Geol. 169, 28–39. https://doi.org/10.1016/j.coal.2016.11.002

Vass, Christopher R., Noble, A., Ziemkiewicz, P.F., 2019. The occurrence and concentration of rare earth elements in acid mine drainage and treatment by-products: Part 1—Initial survey of the northern Appalachian coal basin. Mining, Metall. Explor. 36, 917–929. https://doi.org/10.1007/s42461-019-0097-z

Vass, Christopher R, Noble, A., Ziemkiewicz, P.F., 2019. The Occurrence and Concentration of Rare Earth Elements in Acid Mine Drainage and Treatment Byproducts. Part 2: Regional Survey of Northern and Central Appalachian Coal Basins. Mining, Metall. Explor. 1–13.

Vaziri Hassas, B., Rezaee, M., Pisupati, S. V., 2020. Precipitation of rare earth elements from acid mine drainage by CO2 mineralization process. Chem. Eng. J. 399, 125716. https://doi.org/10.1016/j.cej.2020.125716

683 Verplanck, P.L., Nordstrom, D.K., Taylor, H.E., Kimball, B.A., 2004. Rare earth element partitioning
684 between hydrous ferric oxides and acid mine water during iron oxidation. Appl. Geochemistry
685 19, 1339–1354. https://doi.org/10.1016/j.apgeochem.2004.01.016

686 Wang, X., Jiang, H., Fang, D., Liang, J., Zhou, L., 2019. A novel approach to rapidly purify acid mine
687 drainage through chemically forming schwertmannite followed by lime neutralization. Water
688 Res. 151, 515–522. https://doi.org/10.1016/j.watres.2018.12.052

689 Wang, Y., Gao, B.Y., Xu, X.M., Xu, W.Y., Xu, G.Y., 2009. Characterization of floc size, strength and
690 structure in various aluminum coagulants treatment. J. Colloid Interface Sci. 332, 354–359.
691 https://doi.org/10.1016/j.jcis.2009.01.002

692 Wang, Y., Noble, A., Vass, C., Ziemkiewicz, P., 2021. Speciation of rare earth elements in acid mine
693 drainage precipitates by sequential extraction. Miner. Eng. 168, 106827.
694 https://doi.org/10.1016/j.mineng.2021.106827

695 Webster, J.G., Swedlund, P.J., Webster, K.S., 1998. Trace metal adsorption onto an acid mine
696 drainage iron(III) oxy hydroxy sulfate. Environ. Sci. Technol. 32, 1361–1368.
697 https://doi.org/10.1021/es9704390

698 Wei, X., Viadero Jr, R.C., Buzby, K.M., 2005. Recovery of iron and aluminum from acid mine
699 drainage by selective precipitation. Environ. Eng. Sci. 22, 745–755.

700 Zhang, W., Honaker, R., 2020. Process development for the recovery of rare earth elements and
701 critical metals from an acid mine drainage. Miner. Eng. Minor Revi.

702 Zhang, W., Honaker, R.Q., 2018. Rare earth elements recovery using staged precipitation from a
703 leachate generated from coarse coal refuse. Int. J. Coal Geol. 195, 189–199.
704 https://doi.org/10.1016/j.coal.2018.06.008

705 Zhang, W., Noble, A., Yang, X., Honaker, R., 2020. A comprehensive review of rare earth elements
706 recovery from coal-related materials. Minerals 10, 1–30. https://doi.org/10.3390/min10050451

707 Zhao, F., Cong, Z., Sun, H., Ren, D., 2007. The geochemistry of rare earth elements (REE) in acid

708 mine drainage from the Sitai coal mine, Shanxi Province, North China. Int. J. Coal Geol. 70,
709 184–192. https://doi.org/10.1016/j.coal.2006.01.009
710

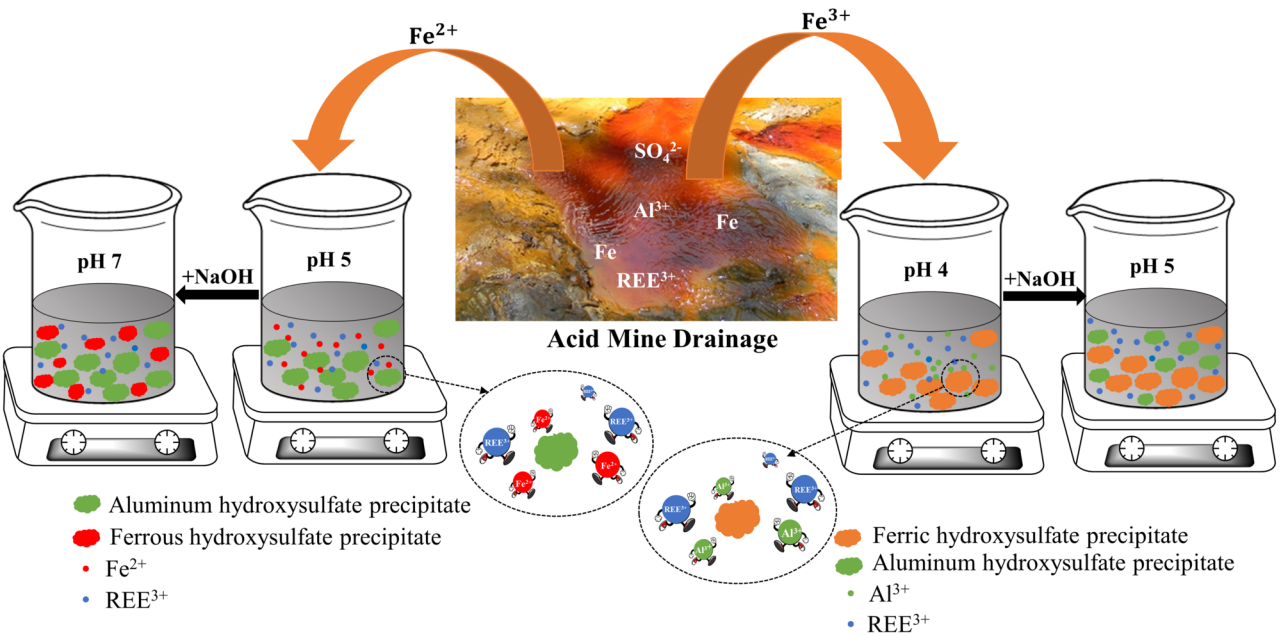
Fe2+
Fe3+
SO4 2-
Al3+
Fe
Fe
REE3+
Acid Mine Drainage
pH 7
+NaOH
pH 5
pH 4
+NaOH
pH 5
Aluminum hydroxysulfate precipitate
Ferrous hydroxysulfate precipitate
Fe2+
REE3+
Ferric hydroxysulfate precipitate
Aluminum hydroxysulfate precipitate
Al3+
REE3+